Modeling of the dynamic contact in stick-slip microdrives using the method of reduction of dimensionality

E. Teidelt*, E. Willert, A.E. Filippov[1], and V.L. Popov

Berlin University of Technology, Berlin, 10623, Germany
[1] Donetsk Institute for Physics and Engineering NASU, Donetsk, 83114, Ukraine

In this work we present a new method to describe movements of stick-slip microdrives. On the microscopic scale we model the contact between actuator and slider as a dynamic tangential contact using the method of reduction of dimensionality. On the macroscopic scale simple one- and three-dimensional equations of motion are derived. An algorithm to solve these equations will be introduced. The results of the simulation will be compared qualitatively and quantitatively to experimental investigations. Even for the simplest assumed model it proves that experimental and numerical values correlate excellently.

Keywords: method of reduction of dimensionality, dynamic tangential contact, stick-slip microdrives

DOI: 10.1134/S1029959912030071

1. Introduction

Positioners and force generating devices in macroscopic and microscopic devices are needed in many technological areas. Stick-slip drives are a commonly used mechanism to precisely position a slider, for example, in atomic force microscopy. However, the physical description of these devices is not yet completely satisfying, since the contact mechanisms between actor and slider are not thoroughly understood. The aim of this work is to introduce a new method to achieve a better understanding of these mechanisms. To do so, we will first introduce the specifically investigated stick-slip microdrive. Then, we will describe a method to model the slider actuator interaction as a dynamic tangential contact by means of the method of reduction of dimensionality. Finally, we will numerically solve the equations of motions of the system and compare the numerical results with the experimental investigations of [1].

2. Stick-slip microdrives

Stick-slip microdrives are devices using stick-slip motion to precisely position a slider or exert forces onto an object. The principle used is simple, hence, mechatronic implementations are relatively easy and diverse. One of the first drives was introduced by Pohl in 1987 (see [2]). Simply speaking, a mass is dragged and released by (piezoelectric) actuators. During the slow motion, the mass sticks to the actuator and is moved forward, whereas during the fast motion of the actuator, the mass slips. Another prominent advantage of these drives is a theoretical infinite forward motion at a very high resolution. In this paper we will discuss a specific model of a stick-slip drive to create forces as introduced in [1–3]. The setup of these microdrives is depicted in Fig. 1.

Six piezo-actuators are used to induce a saw-tooth like movement of six ruby half spheres. These induce a motion on the slider. Edeler introduces three theoretical models [1] to describe the frictional interaction between the spheres and the slider, namely the LuGre model, the elastoplastic model and the CEIM model.

The LuGre model was introduced by scientists from Lund and Grenoble [4]. It combines different aspects of friction in one model, such as Coulombs friction, viscous friction, Stribeck effects and rough surface interactions. However, this model cannot predict the so-called 0-amplitude, which describes the effect of a limiting amplitude of

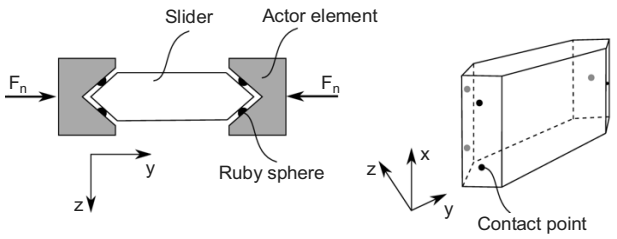

Fig. 1. Schematic view of the stick-slip drive Ramona

* *Corresponding author*
Elena Teidelt, e-mail: elena.teidelt@tu-berlin.de

the displacement of the actuators under which no movement of the slider can be detected and, thus, no force is generated. In [5, 6] an extension of the LuGre-model has been proposed, the elastoplastic model. The idea is, to put it simply, to introduce an additional parameter in order to take an elastic deformation of the contact into account. Again, this model has been revised to accurately predict the influence of the preload and different material parameters. The CEIM-model [1, 3] permits a high qualitative and quantitative agreement between measurements and theory due to six empirical parameters. However, the above theories did not take into account the detailed geometry of the contacts between ruby spheres and the plane slider. In the present paper we show that the experimentally observed results mainly stem just from the properties of the dynamic tangential contact between a sphere and a plane and do not need any sophisticated frictional laws for their description.

3. The dynamic tangential contact and the method of reduction of dimensionality

In this section we will briefly summarize the main governing equations of the dynamic contact with creep (see also [7]). Afterwards, we will describe how the method of reduction of dimensionality may be used to exactly describe the tangential contact.

It is well known that if an elastic sphere is pressed with a normal force

$$F_n = (4/3)E^* R^{1/2} d^{3/2} \tag{1}$$

onto an elastic half-space, the normal pressure is given by the Hertzian equation

$$p = p_0 (1-(r/a)^2)^{1/2}. \tag{2}$$

In Eqs. (1) and (2), $a = \sqrt{Rd}$ is the contact radius, d is the indentation depth, $p_0 = 3/2\, F_n/(\pi a^2)$, and

$$\frac{1}{E^*} = \frac{1-\nu_1^2}{E_1} + \frac{1-\nu_2^2}{E_2} \tag{3}$$

denotes the effective elastic modulus; E_1, E_2, ν_1 and ν_2 are the Young's moduli and Poisson's ratios of the contacting bodies (see, e.g., [7]).

In the presence of tangential forces, tangential stresses will exist in the contact area. Throughout the paper, we assume that at any point inside the contact region, Coulomb's frictional law is valid in its simplest form:

$$\begin{aligned} &\tau \le \mu p, \text{ sticking,} \\ &\tau > \mu p, \text{ sliding,} \end{aligned} \tag{4}$$

where τ is the tangential stress at some point inside the contact region and μ, the coefficient of friction. If a tangential force F_x is increasing, the inner part of the contact region (inside the circle with a radius c) first remains "sticking" to the substrate, while some slip always occurs in the vicinity of the boundary of the contact region (in the area outside the circle with the radius c). The tangential force F_x and the radius of the stick-region are related according to [7] by equation

$$F_x = \mu F_n (1-(c/a)^3). \tag{5}$$

The maximal tangential displacement of the sphere is achieved at the critical force $F_{x,c} = \mu F_n$ when the radius of the sticking region becomes zero ($c = 0$) and is equal to

$$u_{x\max} = \frac{\mu p_0 \pi a}{2G^*} = \frac{3\mu F_n}{4G^* a}. \tag{6}$$

Here G^* is the effective shear modulus defined as

$$\frac{1}{G^*} = \frac{2-\nu_1}{4G_1} + \frac{2-\nu_2}{4G_2}. \tag{7}$$

The solution of a dynamic tangential contact problem is much more complicated and still has not been found in an analytical form. Its numerical simulation (e.g., using the boundary element method) is too time consuming for combining it with a macroscopic simulation of a dynamic system. A breakthrough in computational contact mechanics has been achieved with the invention of the so-called method of reduction of dimensionality [8–10]. It was first introduced for a normal contact of a spherical indenter. Popov and Geike have shown that the initial 3D contact can be mapped to a 1D line consisting of set of independent springs (as shown in Fig. 3). To be equivalent to the initial three-dimensional body, the normal stiffness Δk_z and the tangential stiffness Δk_x of each spring must be chosen according to the following rules:

$$\Delta k_z = E^* \Delta x, \tag{8}$$

$$\Delta k_x = G^* \Delta x, \tag{9}$$

where Δx is the distance between the springs. Furthermore,

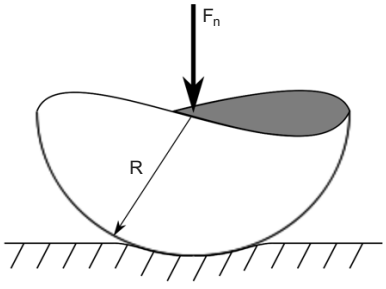

Fig. 2. Hertzian contact between a rigid sphere and an elastic half-space

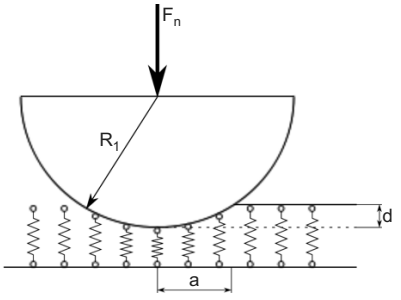

Fig. 3. Elastic foundation equivalent to the Hertzian contact

the radius of the one-dimensional "sphere" R_1 must be chosen according to

$$R_1 = \frac{R}{2}. \tag{10}$$

The solutions of normal contacts with respect to the normal force, indentation depth and contact radius using the method of reduction of dimensionality have been proven to be exact for arbitrary bodies of revolution with and without adhesion [11]. This method has been used in [12, 13] for simulating frictional forces between rough rigid bodies and elastomers and has been extended in [14] to tangential contacts. In this paper, the method of reduction of dimensionality is applied for the modeling of dynamic tangential contacts for the first time in the frame of a hybrid model, combining micro- and macrosimulation into one model.

4. Physical and numerical modeling of the stick-slip drive

The simplest model to describe a force generating stick-slip drive is shown in Fig. 4. The degrees of freedom of the slider are reduced to one translational motion and the six actuators are replaced by one central actuator.

The ruby sphere follows a saw-tooth displacement x_s. The coordinate x describes the displacement of the slider with mass m. The generating force is applied to a wall via a force sensor with stiffness k. Newton's second law then yields

$$m\ddot{x} = -kx + F_r, \tag{11}$$

where F_r is the friction force between sphere and slider. The challenging part is the computation of the friction force, if we model the contact via the method of reduction of dimensionality as described in section 3. Solving the differential equation in each time step, the sphere and the slider, and thus, all springs, undergo a horizontal relative displacement $u_x = x - x_s$. One has to consider the stick or slip state of each spring. Say u_z is the displacement of each spring in the vertical direction, the spring forces are $f_x = \Delta k_x u_x$ and $f_z = \Delta k_z u_z$. A spring undergoes slip if the slip condition

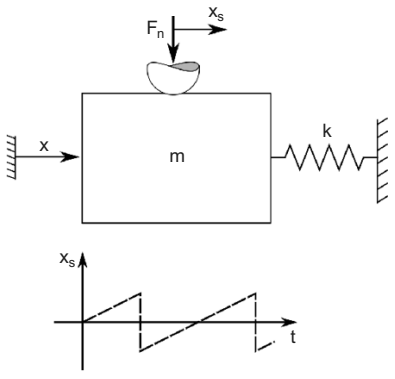

Fig. 4. Simple one-dimensional model of a stick-slip drive

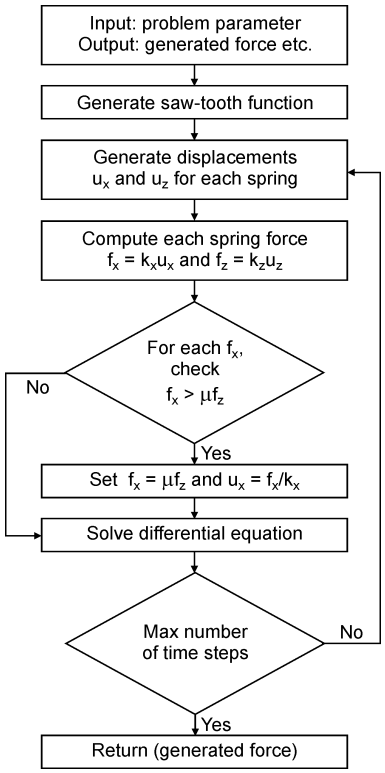

Fig. 5. Algorithm for the implementation of the contact between slider and ruby half-sphere

no longer holds: $f_x = \Delta k_x u_x > \mu f_z$. This implies that for each time step, the condition of each spring must be computed. An algorithm could be implemented as introduced in Fig. 5.

The above model can be enhanced if the reduction of contact points is changed as depicted in Fig. 6. Instead of one central contact point, the slider is moved by three ruby spheres in the horizontal direction. This model is unmistakably closer to the genuine model, especially since it takes the symmetry of the actuators into account. The numerical enhancement from three contact points to six contact points is trivial, if the geometrical set-up as depicted in Fig. 1 is

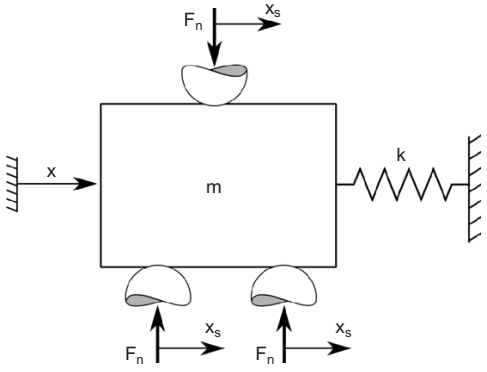

Fig. 6. One-dimensional model of the stick-slip drive with three contact points

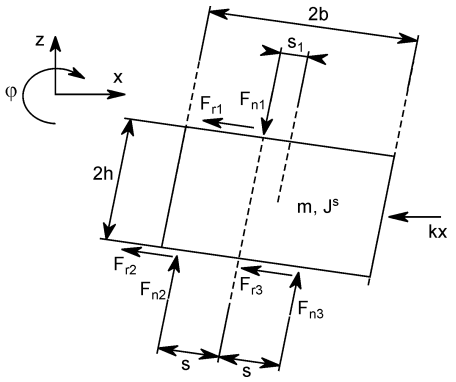

Fig. 7. Free body diagram of a three-dimensional model of the stick-slip drive with three contact points

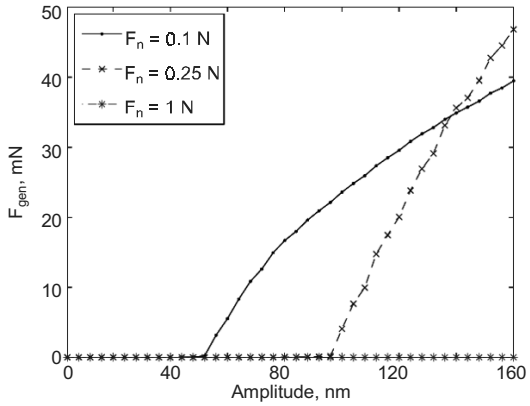

Fig. 9. Maximum generated force with respect to the actuator amplitude for the model with one degree of freedom and one contact point

neglected and the reduction method is used. The results will also be presented in the next section.

However, all considered models still only examine sliding in the horizontal direction, no rotational or vertical movements of the slider are simulated, even though they are clearly detectable in the experiments. Consequently, we implemented a three-dimensional planar model, whose free body diagram is depicted in Fig. 7. Here, x and z are the center of mass coordinates and φ is the rotation angle. The upper sphere is positioned in the middle of the lower spheres, and we assume that the actuators can be controlled such that they perform a synchronic saw-tooth motion.

Furthermore, we assume small movements in z and φ. This yields the following linearized equations of motion:

$$\begin{aligned} -m\ddot{x} &= F_{r1}+F_{r2}+F_{r3}+(F_{n1}-F_{n2}-F_{n3})\varphi+kx,\\ m\ddot{z} &= (F_{r1}+F_{r2}+F_{r3})\varphi-(F_{n1}-F_{n2}-F_{n3}),\\ J^s\ddot{\varphi} &= -(F_{r1}-F_{r2}-F_{r3})h-(F_{n3}-F_{n2})s-\\ &\quad -(F_{n1}-F_{n2}-F_{n3})s_1+kxb\varphi. \end{aligned} \tag{12}$$

In the next section, we will compare the numerical findings for all models along with the measured data presented in [1].

5. Comparison of numerical and experimental results

As an example, we will demonstrate the quality of our numerical results by comparing the results of numerical simulations with experimental results of [1] reproduced in Fig. 8.

The graphs indicate two important characteristics. First, the 0-amplitude is clearly distinguishable. This amplitude increases with rising normal force, since the maximal displacement of the sphere without creep is getting larger as the normal force increases. In addition, we can see that the generated force reaches a saturated level for large enough amplitudes.

In Figs. 9–12 the numerical results for all models are presented. The material and geometrical data used for the simulation are those described in [1] and are listed in Table 1.

It is clearly visible that all graphs can predict the overall tendencies of the generated force regarding the 0-amplitude and the saturation of the forces. Note that all graphs are created without fitting parameters; only the material and geometrical data of [1] are used.

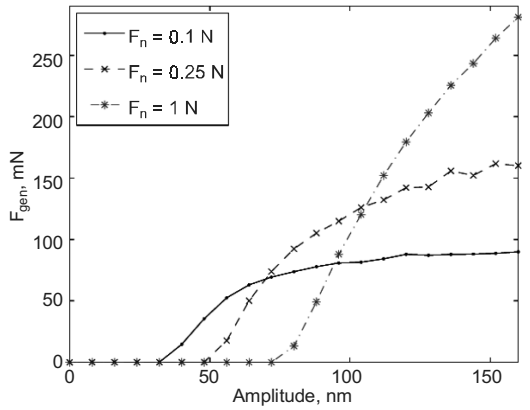

Fig. 8. Maximum generated force with respect to the actuator amplitude, publication kindly permitted by the author of [1]

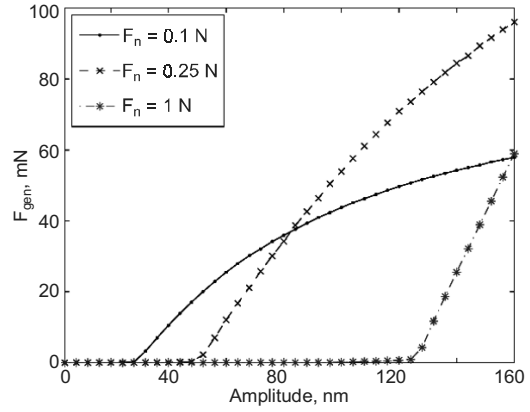

Fig. 10. Maximum generated force with respect to the actuator amplitude for the model with one degree of freedom and three contact points

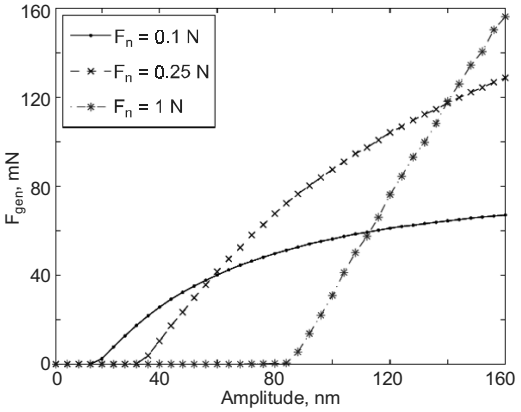

Fig. 11. Maximum generated force with respect to the actuator amplitude for the model with one degree of freedom and six contact points

Furthermore, with increasing the number of contact points for the one-dimensional models, the order of magnitude of the generated force and the 0-amplitude adapts to the measured values. However, the 0-amplitude is not accurately matched. While for one contact point the 0-amplitude tends to be too large, the amplitudes for the small forces and the remaining one-dimensional models do not agree with the experimental data. An explanation for this circumstance may be that the contact is modeled as a smooth rigid sphere, pressed into an elastic half-space. Even though the real ruby half-spheres are small, the microscopic contact will be much better described as a rough surface.

For the three-dimensional model, the results imply that the vertical and rotational degree of freedom do not overly influence the force generation, compared with the one-dimensional model with three contact points. A detailed observation of z and φ indeed shows that these coordinates quickly reach a saturated level and a further movement is only possible in the horizontal direction x.

One important observation can additionally be made. For a change in the normal force F_n by the factor κ, the 0-amplitude changes by a factor $\alpha \approx \kappa^{2/3}$. If we recall that the maximum displacement of the sphere and the normal force are related by $u_{x\max} \approx F_n^{2/3}$, consideration of a dimensionless plot seems necessary and is given in Fig. 13.

The 0-amplitude agrees nicely with the maximum displacement of the sphere before slipping occurs. Additionally, we can see that the maximum generated force is limited by the static friction force μF_n between slider and actuator.

Table 1

Material and geometrical data used for the numerical simulation

Steel Young's modulus E_1, GPa	200
Ruby Young's modulus E_2, GPa	370
Poisson's ratio ν_1, ν_2	0.3
Friction coefficient μ	0.3
Radius of the ruby sphere, mm	0.5
Mass of the slider m, g	3
Mass moment of inertia J^s, g·mm^2	66.5

6. Summary

In the present work, we proposed a new theoretical and numerical approach to describe the contact mechanisms of stick-slip microdrives, namely the method of reduction of dimensionality. Based on the classical tangential contact theory, an efficient algorithm is developed. The quality of the algorithm and the new microscopic method is proven by a stepwise improvement of the macroscopic model of the microdrive. Not only a qualitative agreement between numerical evaluation and experiments is reached, but without any fitting parameters, all fundamental values, such as the generated force and the 0-amplitude, are of the same magnitude as the experimental data. Finally a master curve is found which may be used to characterize all load cases. In the future, it would be interesting to investigate if a more precise description is possible by a combination of the macroscopic description provided in this work with models for atomic scale actuators [15].

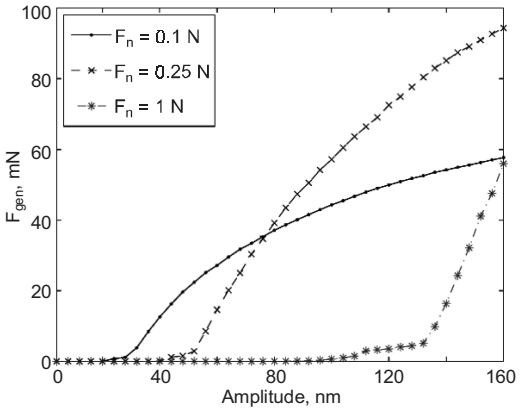

Fig. 12. Maximum generated force with respect to the actuator amplitude for the model with three degrees of freedom and three contact points

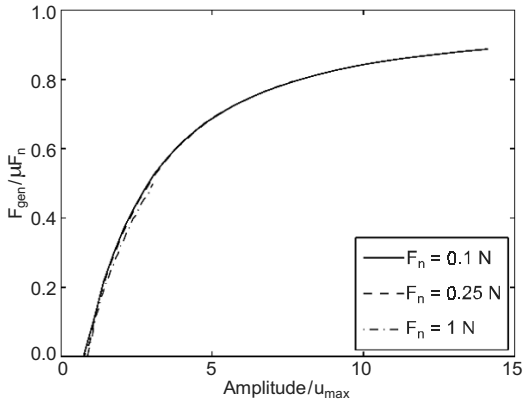

Fig. 13. Scaled graph of the generated force with respect to the amplitude for the one-dimensional model with one contact point

Useful discussions with C. Edeler and S. Fatikow are gratefully acknowledged. A.E. Filippov acknowledges financial support of the Deutsche Forschungsgemeinschaft.

References

[1] C. Edeler, Modellierung und Validierung der Krafterzeugung mit Stick-Slip-Antrieben für nanorobotische Anwendungen, Verl. Dr. Hut, München, 2011.

[2] D.W. Pohl, Dynamic piezoelectric translation devices, Rev. Sci. Instrum., 58, No. 1 (1987) 54.

[3] C. Edeler, I. Meyer, and S. Fatikow, Modeling of stick-slip microdrives, J. Micro-Nano Mechatronics, No. 3–4 (2011) 65.

[4] C. Canudas de Wit, H. Olsson, K.J. Astrom, and P. Lischinsky, A new model for control of systems with friction, IEEE T. Automat. Contr., 40, No. 3 (1995) 419.

[5] P. Dupont, V. Hayward, B. Armstrong, and F. Altpeter, Single state elastoplastic friction models, IEEE T. Automat. Contr., 47, No. 5 (2002) 787.

[6] P. Dupont, B. Armstrong, and V. Hayward, Elasto-plastic friction model: contact compliance and stiction, Proc. 2000 Amer. Control. Conf., 2 (2000) 1072.

[7] V. Popov, Contact Mechanics and Friction: Physical Principles and Applications, Springer, Berlin, 2010.

[8] V.L. Popov and S.G. Psakhie, Numerical simulation methods in tribology, Tribol. Int., 40, No. 6 (2007) 916.

[9] T. Geike and V.L. Popov, Mapping of three-dimensional contact problems into one dimension, Phys. Rev. E, 76 (2007) 036710.

[10] T. Geike and V.L. Popov, Reduction of three-dimensional contact problems to one-dimensional ones, Tribol. Int., 40, No. 6 (2007) 924.

[11] M. Heß, Über die exakte Abbildung ausgewählter dreidimensionaler Kontakte auf Systeme mit niedrigerer räumlicher Dimension, Cuvillier-Verlag, Göttingen, 2011.

[12] V.L. Popov and A.E. Filippov, Force of friction between fractal rough surface and elastomer, Tech. Phys. Lett., 36, No. 9 (2010) 525.

[13] V.L. Popov and A. Dimaki, Using hierarchical memory to calculate friction force between fractal rough solid surface and elastomer with arbitrary linear rheological properties, Tech. Phys. Lett., 37 (2011) 8.

[14] V.L. Popov, Basic ideas and applications of the method of reduction of dimensionality in contact mechanics, Phys. Mesomech., 15, No. 5–6 (2012) 254.

[15] V.L. Popov, Nanomachines: Methods of induce a directed motion at nanoscale, Phys. Rev. E, 68 (2003) 026608.